

**Temperature lidar
measurements**

M. Alpers et al.

Temperature lidar measurements from 1 to 105 km altitude using resonance, Rayleigh, and Rotational Raman scattering

M. Alpers*, R. Eixmann, C. Fricke-Begemann, M. Gerding, and J. Höffner

Leibniz-Institute of Atmospheric Physics, Kühlungsborn, Germany

* now at German Aerospace Center (DLR), Space Management, Earth Observation Division, Bonn, Germany

Received: 12 December 2003 – Accepted: 21 January 2003 – Published: 6 February 2004

Correspondence to: M. Gerding (gerding@iap-kborn.de)

Title Page

Abstract

Introduction

Conclusions

References

Tables

Figures

◀

▶

◀

▶

Back

Close

Full Screen / Esc

Print Version

Interactive Discussion

© EGU 2004

Abstract

For the first time, three different temperature lidar methods are combined to obtain time-resolved complete temperature profiles with high altitude resolution over an altitude range from the planetary boundary layer up to the lower thermosphere (about 1–105 km). The Leibniz-Institute of Atmospheric Physics (IAP) at Kühlungsborn, Germany (54° N, 12° E) operates two lidar instruments, using three different temperature measurement methods, optimized for three altitude ranges: (1) Probing the spectral Doppler broadening of the potassium D₁ resonance lines with a tunable narrow-band laser emitter allows the determination of atmospheric temperature profiles at the metal layer altitudes (80–105 km). (2) Between about 20 and 90 km, temperatures were calculated from Rayleigh backscattering on air molecules, where the upper start values for the calculation algorithm were taken from the potassium lidar results. Correction methods have been applied to account for, e.g. Rayleigh extinction or Mie scattering of aerosols below about 32 km. (3) At altitudes below about 25 km, backscattering on the Rotational Raman lines is strong enough to obtain temperatures by measuring the temperature dependent spectral shape of the Rotational Raman spectrum. This method works well down to about 1 km. The instrumental configuration of the IAP lidars was optimized for a 3–6 km overlap of the temperature profiles at the method transition altitudes. First night-long measurements show clear wave structures propagating from the lower stratosphere up to the lower thermosphere in most of the nights.

1. Introduction

The knowledge of the temporal and spatial structure of the temperature of the Earth's atmosphere over a wide vertical range is essential for the understanding of the Earth's climate. Sporadic measurements of single temperature profiles are insufficient for a realistic observational coverage of the temperature structure. Dynamical processes such as tidal, planetary and gravity waves strongly influence the temperature profile from

Temperature lidar measurements

M. Alpers et al.

Title Page

Abstract

Introduction

Conclusions

References

Tables

Figures

◀

▶

◀

▶

Back

Close

Full Screen / Esc

Print Version

Interactive Discussion

**Temperature lidar
measurements**M. Alpers et al.

[Title Page](#)[Abstract](#)[Introduction](#)[Conclusions](#)[References](#)[Tables](#)[Figures](#)[◀](#)[▶](#)[◀](#)[▶](#)[Back](#)[Close](#)[Full Screen / Esc](#)[Print Version](#)[Interactive Discussion](#)

© EGU 2004

the troposphere up to the upper mesosphere and thermosphere. The vertical propagation range and the change in the properties of these waves (wavelength, amplitude, etc.) are still under scientific discussion. The experimental analysis of these dynamical processes in the Earth's atmosphere requires continuous observations with good temporal and vertical resolution. To cover the wide vertical propagation range of these waves including the formation and breaking altitudes the complete lower and middle atmosphere from ground to about 100 km must be observed. Wave parameter inversion methods require data sets of high spatial and temporal resolution and extended as far as possible (see, e.g. review by Fritts and Alexander, 2003).

Presently, there exists no in-situ or remote sensing experimental method, which covers the full altitude range from the ground up to the lower thermosphere. Dependent on their specific methods, the measurements are limited to small altitude ranges. Only the combination of different methods allows measurements of complete temperature profiles over a wider altitude range. To avoid systematic errors, the observation geometry and time scales of the combined methods should be as similar as possible. It is problematic to combine methods with strongly different time scales (e.g. a rocket-borne in-situ measurement of a few minutes duration with a 1 h lidar measurement) or different measurement geometry (e.g. a space-borne limb-scanning spectrometric measurement with a local lidar measurement).

In this work we describe a combination of different ground-based temperature lidar methods, which allows measurements of complete temperature profiles between altitudes of 1 and 105 km. The lidars of the Leibniz Institute of Atmospheric Physics (IAP) at Kühlungsborn, Germany (54° N, 12° E) use three different scattering types for temperature measurements:

1. Resonance scattering: In the altitude range between 80 and 105 km there exist layers of free metal atoms, as e.g. Fe, Ca, Na, and K. Probing the spectral Doppler broadening of the metal resonance lines, especially Na-D₂ and K-D₁, with tunable narrow-band laser emitters allows the determination of atmospheric temperature profiles at the metal layer altitudes (e.g. Fricke and von Zahn, 1985; von Zahn and Höffner,

1996).

2. Rayleigh scattering: In the absence of resonance and particle scattering, atmospheric temperatures can be calculated from the density profiles obtained from the Rayleigh backscatter signal (e.g. Hauchecorne and Chanin, 1980). Owing to the exponential decrease of the Rayleigh backscatter signal with altitude, this method is limited to altitudes below about 90 km. For temperature retrieval, the “top-to-bottom“ integration method needs a temperature start value at the top of the profile. For a stand-alone Rayleigh lidar this value can only be estimated from model atmospheres with large uncertainties (about ± 30 K). In case of the availability of a metal resonance lidar the uncertainty of the start value can be significantly reduced to less than ± 5 K and the temperature calculation from the Rayleigh backscatter signal can be extended to higher altitudes. The IAP operates a Rayleigh/Mie/Raman (RMR) lidar at Kühlungsborn, which is capable for Rayleigh temperature measurements (Alpers et al., 1999).

3. Rotational Raman scattering: Mie scattering on aerosols prevents temperature measurements with the Rayleigh method below about 20 km. At these low altitudes, backscattering at the Rotational Raman lines of the air molecules is strong enough to obtain temperatures by measuring the temperature dependent spectral shape of the Rotational Raman spectrum. In practice, two parts of the Rotational Raman spectrum are measured, using two interference filters of about 0.4–0.5 nm spectral width and about 1 nm spectral distance in the lidar detector. The temperature at a specific altitude can be calculated from the ratio of the backscatter signals, obtained at these two wavelengths. This requires a signal-ratio-to-temperature calibration, which can be delivered by simultaneous in-situ radiosonde temperature measurements or by highly accurate measurements of the spectral shapes of the two filters and the detector sensitivities. The second method is applied at the IAP (see below) and described in detail by Vaughan et al. (1993). An alternative approach to the rotational Raman method was published by Behrendt and Reichardt (2000).

The three described temperature lidar methods on their own are experimentally well established and are utilized in various lidar systems all over the world. Com-

Temperature lidar measurements

M. Alpers et al.

Title Page

Abstract

Introduction

Conclusions

References

Tables

Figures

◀

▶

◀

▶

Back

Close

Full Screen / Esc

Print Version

Interactive Discussion

binning sodium resonance and Rayleigh temperature soundings between about 25 and 103 km was previously reported by Dao et al. (1995) on a single night. But, at the IAP K hlungsborn, for the first time all three methods are combined for complete temperature measurements covering the whole altitude range from the planetary boundary layer up to the lower thermosphere (about 1–105 km).

2. Instruments and observation methods

The technical setups of the IAP lidar instruments are described in detail in previous publications (von Zahn and H ffner, 1996; Alpers et al., 1999). In this work only setup changes in the configurations or technical aspects are discussed, which are essential for the temperature measurements. The two lidar systems are technically independent.

Potassium lidar: In addition to the transportable potassium resonance lidar described by von Zahn and H ffner (1996), the IAP has operated a stationary system since 2002 in the institute building at K hlungsborn, Germany. Both systems have the same operation principle of scanning the K-D₁ line at 770 nm. Dependent on the vertical extension of the potassium layer, temperature profiles with errors less than 10% can be obtained between about 80 and 105 km with an integration of 1 h and a 2 km altitude resolution. The lidar detector is equipped with a narrow-band potassium Faraday Anomalous Dispersion Optical Filter (FADOF) to facilitate daytime measurements (Fricke-Begemann et al., 2002).

RMR lidar: The IAP operates a Rayleigh/Mie/Raman (RMR) lidar at K hlungsborn, with a three wavelengths laser emitter. For temperature measurements only the second and third fundamental Nd:YAG laser wavelengths (532 nm and 355 nm) are relevant. The system has been described in detail by Alpers et al. (1999), but since then, the detector system of the RMR lidar has been completely re-arranged as shown in Fig. 1. The detectors of the 532 nm wavelength were optimized for Rayleigh temperature measurements in the stratosphere and mesosphere. For Rayleigh temperature measurements at high altitudes, a new high sensitivity photomultiplier (HSPMT, Hama-

Title Page

Abstract

Introduction

Conclusions

References

Tables

Figures

⏪

⏩

◀

▶

Back

Close

Full Screen / Esc

Print Version

Interactive Discussion

Temperature lidar measurementsM. Alpers et al.

[Title Page](#)[Abstract](#)[Introduction](#)[Conclusions](#)[References](#)[Tables](#)[Figures](#)[I◀](#)[▶I](#)[◀](#)[▶](#)[Back](#)[Close](#)[Full Screen / Esc](#)[Print Version](#)[Interactive Discussion](#)

© EGU 2004

matsu type H7421-40) was added to the 532 nm (high) detection branch. Its quantum efficiency at this wavelength is about a factor two higher than that of standard photo-multipliers (PMTs). A motorized mirror mount allows automatic switching between the two PMTs. This new HSPMT and the combination of four 50-cm receiving telescopes (total effective diameter: 100 cm) for the Rayleigh detector allows temperature measurements up to 90 km altitude within 1 h integration time, 1 km altitude resolution, and with a statistical temperature error of less than 10%. Dependent on weather conditions and on the vertical extension of the potassium layer, the vertical overlap between the resonance and the Rayleigh temperature profiles is about 1–5 km.

Due to the limited dynamic range of PMTs, the Rayleigh backscatter signal must be blocked below 40 km altitude by a rotating chopper wheel, which is synchronized with the laser pulse emission. A second detector for the wavelength 532 nm with a separate receiving telescope (50 cm diameter) and with another blocking time characteristic covers the altitude range between about 20 and 50 km. For temperature calculations from this low altitude signal, the temperature values of the high altitude Rayleigh detector are used as upper start values. Both Rayleigh temperature profiles together cover the altitude range 20–90 km and have, dependent on weather conditions, a vertical overlap of about 5–10 km.

For the high altitude range, Rayleigh temperature measurements are also possible with the UV detector (355 nm (high), see Fig. 1). This detector is equipped with a standard PMT, which has a much lower dead time than the HSPMT at 532 nm. Therefore, the UV data is used for exact determination and from time to time for control of the dead time correction factor of the HSPMT at high count rates only.

The Rotational Raman detector of the IAP RMR lidar uses a sixth receiving telescope (50 cm diameter) and has no mechanical chopper (see Fig. 1). To prevent PMT overload, the backscatter signal is attenuated by about one order of magnitude. Presently, the detector contains only one PMT and a motorized IF filter wheel, which alternates between the two Rotational Raman filters every 4000 laser pulses (about 2.2 min). This configuration does not require PMT sensitivity calibration, but allows temperature

**Temperature lidar
measurements**M. Alpers et al.

[Title Page](#)[Abstract](#)[Introduction](#)[Conclusions](#)[References](#)[Tables](#)[Figures](#)[◀](#)[▶](#)[◀](#)[▶](#)[Back](#)[Close](#)[Full Screen / Esc](#)[Print Version](#)[Interactive Discussion](#)

© EGU 2004

measurements only for temporal stable atmospheric transmission conditions. For example, passing low tropospheric clouds prevent Rotational Raman temperature measurements with this detector configuration because here atmospheric transmission becomes time-dependent. Therefore, the Rotational Raman detector of the IAP RMR lidar will be modified for simultaneous Rotational Raman operation in the future. We use the filter calibration method described by Vaughan et al. (1993) and the quantum physical constants given there and by Butcher et al. (1971) and Arshinov et al. (1983). Additionally we launch radiosondes for control purposes on special occasions. With 1 h integration, temperature measurements up to 26 km are possible with a vertical resolution of 1 km and a temperature error of less than 10%. The Rotational Raman method works well down to about one kilometer altitude, where the backscatter signals become too weak due to the geometric overlap function (bistatic system) and defocusing of the receiving telescope (limited depth of focus).

On its way through the atmosphere the emitted laser light is affected by various extinction processes: (1) Rayleigh scattering has a nearly homogeneous phase function, which reduces significantly the transmission in beam direction. The process is dependent on the number density of the air molecules and has a strong wavelength characteristic ($\sim\lambda^{-4}$). We use the Rayleigh scatter cross sections of Thome et al. (1999) and air molecule number densities calculated from the corresponding zonal and monthly mean CIRA model profile (Fleming et al., 1990). By correcting the signal for the Rayleigh extinction the calculated temperature decreases by about 1 K or less for altitudes of 20–30 km or above, respectively. (2) Ozone significantly absorbs light in the UV below about 350 nm (Huggins bands) and the visible region between about 430 and 850 nm (Chappuis bands). For our ozone absorption correction we use the O₃ absorption cross section from Bogumil et al. (2003) and mean ozone profiles from the “Berliner Ozon-Modell” (Fortuin and Langematz, 1994). The ozone correction amounts to about 3 K in the maximum altitude of the O₃ layer. (3) Above the troposphere and below about 35 km altitude Mie scattering on stratospheric aerosols can significantly affect the backscatter signal. The number density within these aerosol layers is low enough

**Temperature lidar
measurements**M. Alpers et al.

to neglect extinction (except for periods after strong volcano eruptions as Mt. Saint Helens or Pinatubo), but the enhanced backscattering has to be considered. Unfortunately, neither the vertical number density profile nor the composition of these stratospheric particles (i.e. their backscatter parameters) is known well enough for an exact backscatter ratio correction. For a rough compensation of the aerosol backscattering we introduce a mean aerosol layer with a backscatter ratio R of 1.06 below 28 km altitude and decreasing to 1.00 above (<28 km: 1.06, 28–29 km: 1.05, 29–30 km: 1.04, 30–31 km: 1.03, 31–32 km: 1.02, >32 km: 1.00). These numbers are comparable (though more conservative) to the values of Fujiwara et al. (1982) and Zuev et al. (2001), who describe R numbers of up to 1.1 at 28–30 km altitude for volcanic-free conditions.

The aerosol correction affects the temperatures by up to 8 K around 28 km. We are aware of the uncertainties of this procedure, but comparisons of the corrected Rayleigh temperature profiles with the Rotational Raman and radiosonde data show that the results are close to reality. Nevertheless, to avoid this uncertainty in future, the IAP RMR lidar will be equipped with a vibrational Raman channel (which is not influenced by Mie backscattering) and/or a high Rotational Raman channel for the altitude region 15–40 km.

With the three methods described, complete temperature profiles between 1 and 105 km altitude can be obtained. The methods have identical time scales, observation geometries, vertical resolutions, and temperature errors (1 h integration time, about 0.5 mrad field of view (FOV), 1 km vertical resolution, and less than 10% temperature error). This allows the determination of wave parameters from a large fraction of the planetary, tidal, or gravity wave scale.

Currently, the combined temperature measurements are limited to the nighttime. Daytime filtering for the individual lidars is possible and already realized for the IAP potassium resonance lidar (Fricke-Begemann et al., 2002). In general, the current solar background reduction techniques (FADOF, high resolution Fabry-Perot etalons, etc.) are not effective enough to allow calculations of vertically overlapping temperature pro-

[Title Page](#)[Abstract](#)[Introduction](#)[Conclusions](#)[References](#)[Tables](#)[Figures](#)[I◀](#)[▶I](#)[◀](#)[▶](#)[Back](#)[Close](#)[Full Screen / Esc](#)[Print Version](#)[Interactive Discussion](#)

© EGU 2004

files during daytime.

3. Measurements and results

Figure 2 shows an example of raw backscatter profiles, obtained by the IAP lidars (panel a), and temperature profiles (panels b+c), calculated from these data. The profiles of the different methods have altitude overlaps of a few kilometers with their neighbors. Additionally, the corresponding zonal and monthly mean CIRA model profile is plotted (Fleming et al., 1990). The statistical temperature errors of the different methods vary with altitude: The temperature profile of the potassium resonance lidar has small errors (less than 1 K) around the center of the metal layer near 90 km and increasing errors at its bottom and top. Due to the exponential decrease of the Rayleigh backscatter signals with altitude, the Rayleigh temperature errors are small at the bottom of the profiles (less than 1 K) and increase with altitude. The situation is similar for the Rotational Raman temperature profile. Temperature values with more than 10 K uncertainty are discarded, leaving a reliable continuous temperature profile from 1 to 105 km.

Figure 2b includes the temperature profile calculated from the 355 nm (high) data (blue curve). Due to the lower sensitivity of the UV-branch the temperature profile is limited to an upper altitude of about 76 km. At an altitude of 42 km, the UV data is used for the exact determination of the dead time correction factor for the HSPMT. Due to the exponential altitude dependence of the Rayleigh backscatter signal the temperature results at 532 nm are dependent on this parameter only for the lowest 5 km range (<47 km). Above, for the HSPMT the dead time correction is much lower than 1%. Therefore, the good agreement between the 355 nm (high) and the 532 nm (high) results over the whole altitude range demonstrates the stability of the temperature calculation algorithm and the high data quality.

Figure 2c shows a subrange of the temperature profiles in Fig. 2b (low Rayleigh and Rotational Raman) but only below 40 km altitude together with temperature data

Temperature lidar measurements

M. Alpers et al.

Title Page

Abstract

Introduction

Conclusions

References

Tables

Figures

◀

▶

◀

▶

Back

Close

Full Screen / Esc

Print Version

Interactive Discussion

**Temperature lidar
measurements**M. Alpers et al.

[Title Page](#)[Abstract](#)[Introduction](#)[Conclusions](#)[References](#)[Tables](#)[Figures](#)[◀](#)[▶](#)[◀](#)[▶](#)[Back](#)[Close](#)[Full Screen / Esc](#)[Print Version](#)[Interactive Discussion](#)

© EGU 2004

from a simultaneous radiosonde launched at Kühlungsborn and with data from two radiosondes launched at 22h UT at the closest German Weather Service (DWD) stations at Schleswig and Greifswald (located about 100 km east and west of Kühlungsborn). Due to the limited ascent rate of a balloon-borne radiosonde (about 5 m/s) its profile in principle consists of data measured at different times (data at the burst altitude are obtained about 2 h later than data obtained on ground). Because we want to compare the Rayleigh lidar data with the radiosonde, in Figs. 2b and 2c we chose the lidar profile obtained during the second half of the radiosonde flight period, when the balloon was above 15 km. Below about 33 km the aerosol and extinction corrected Rayleigh temperature profile fits well to the radiosonde data, indicating the importance of the various corrections. Radiosonde and rotational Raman lidar temperature profiles agree well within their experimental errors.

The measured temperature lidar profile of Fig. 2b shows a good agreement with the CIRA model values at troposphere and lower stratosphere altitudes, but large deviations at upper stratosphere (about 20 K) and mesopause altitudes (up to 50 K!). These differences are caused by the different spatial and temporal basics of the two data sets: While the CIRA profile represents a monthly zonal mean with 10° latitude grid, the lidar profile is a local snapshot of the atmospheric temperature structure. The temperature profile of Fig. 2b shows clear wave structures with about 10–12 km vertical wavelength above 50 km altitude. At lower altitudes no clear wave structures are present. Short time processes such as wave structures and warming or cooling processes at hourly or daily scales strongly influence the local vertical structure of the temperature profile but are smoothed out in the zonal monthly mean profile of the CIRA model atmosphere.

The excellence of long-range and continuous night-time temperature lidar measurements becomes obvious with demonstrating the time dependence of the temperature profile and clearly illustrating vertical wave structures. Figure 3 shows the color-coded temperature deviation from mean from 1 to 110 km altitude, measured with the IAP lidars at Kühlungsborn during 36 h on 22–24 February 2003. The deviation is calculated as follows: For each altitude bin a mean temperature is calculated from the observed

**Temperature lidar
measurements**M. Alpers et al.

profiles. This value is subtracted from the absolute temperature values for each time step. At altitude ranges of temperature profile overlap between two methods, the values with the lower temperature errors are used. Only temperature values with less than 10 K error are considered at all. The different observation periods of potassium lidar and RMR lidar may result in phase shifts of the temperature variation. In order to avoid phase jumps around 80 km altitude, the mean profile is calculated only for simultaneous sounding times, accepting that this 12-h-mean may differ slightly from the daily mean in the potassium layer height.

Clear wave structures with downward propagating phase with about 10–20 km vertical wavelength and 9–14 h period appear above 40 km altitude. Only below about 20 km the variability is partly caused by noise. Due to the daytime operation capability of the potassium resonance lidar the wave structure at the 90 km altitude range is detected for the whole 36 h period. The high solar background signal decreases the usable altitude range of the potassium resonance lidar data to less than 10 km during daytime. As explained above, Rayleigh and Rotational Raman measurements are limited to the nighttime.

The data of the Figs. 2 and 3 is part of a five days continuous run from 22 to 27 February 2003. The complete data set will be analyzed in detail in a later publication including analytical wave parameter determination.

In this paper we have demonstrated using time resolved lidar backscatter data to retrieve continuous temperature profiles from close to the ground up to about 105 km. While other methods for “quasi-continuous” temperature profiles combine different techniques and sounding methods, at the IAP we have assembled only lidar data obtained at the same location, but from different types of backscatter. The resolution in time is 1 h or better in all altitudes, allowing for gravity and tidal wave studies. Currently, continuous temperature soundings are limited to the nighttime, although 24-h-measurements are desirable, e.g. for the examination of diurnal and semidiurnal tides. At present, daytime lidars cover only the mesopause region down to about 85 km or the stratosphere and lower mesosphere up to about 65 km. Future lidar technique

[Title Page](#)[Abstract](#)[Introduction](#)[Conclusions](#)[References](#)[Tables](#)[Figures](#)[I◀](#)[▶I](#)[◀](#)[▶](#)[Back](#)[Close](#)[Full Screen / Esc](#)[Print Version](#)[Interactive Discussion](#)

© EGU 2004

developments are required to close this gap.

Acknowledgements. We thank T. Köpnick from the IAP Kühlungsborn for his assistance with the development and construction of our lidar instruments. Schleswig and Greifswald radiosonde data have been made available from the Met Office Global Radiosonde Data set through the British Atmospheric Data Center.

References

- Alpers, M., Eixmann, R., Höffner, J., Köpnick, T., Schneider, J., and von Zahn, U.: The Rayleigh-Mie-Raman lidar at IAP Kühlungsborn, *J. Aerosol Sci.*, 30, Suppl. 1, 637–638, 1999.
- Arshinov, Yu. F., Bobrovnikov, S. M., Zuev, V. E., and Mitev, V. M.: Atmospheric temperature measurements using a pure rotational Raman lidar, *Appl. Opt.*, 22, 2984–2990, 1983.
- Behrend, A. and Reichardt, J.: Atmospheric temperature profiling in the presence of clouds with a pure rotational Raman lidar by use of an interference-filter-based polychromator, *Appl. Opt.*, 39, 1372–1378, 2000.
- Bogumil, K., Orphal, J., Homann, T., Vogt, S., Spietz, P., Fleischmann, O. C., Vogel, A., Hartmann, M., Bovensmann, B., Frerick, J., and Burrows, J. P.: Measurements of molecular absorption spectra with the SCIAMACHY pre-flight model: instrument characterization and reference data for atmospheric remote-sensing in the 230–2380 nm region, *J. Photchem. Photobiol. A*, 6271, 1–18, 2003.
- Butcher, R. J., Willetts, D. V., and Jones, W. J.: On the use of a Fabry-Perot etalon for the determination of rotational constants of simple molecules – the pure rotational Raman spectra of oxygen and nitrogen, *Proc. R. Soc. London Ser. A*, 324, 231–245, 1971.
- Dao, P. D., Farley, R., Tao, X., and Gardner, C. S.: Lidar observations of the temperature profile between 25 and 103 km: evidence for strong tidal perturbation, *Geophys. Res. Lett.*, 22, 2825–2828, 1995.
- Fleming, E. L., Chandra, S., Barnett, J. J., and Corney, M.: Zonal mean temperature, pressure, zonal wind, and geopotential height as functions of latitude, *Adv. Space Res.*, 10, 11–59, 1990.
- Fortuin, J. P. F. and Langematz, U.: An update on the global ozone climatology and on concurrent ozone and temperature trends, *SPIE, Atmospheric Sensing and Modeling*, 2311, 207–216, 1994.

Temperature lidar measurements

M. Alpers et al.

Title Page

Abstract

Introduction

Conclusions

References

Tables

Figures

◀

▶

◀

▶

Back

Close

Full Screen / Esc

Print Version

Interactive Discussion

**Temperature lidar
measurements**

M. Alpers et al.

Title Page

Abstract

Introduction

Conclusions

References

Tables

Figures

◀

▶

◀

▶

Back

Close

Full Screen / Esc

Print Version

Interactive Discussion

© EGU 2004

Fricke, K. H. and von Zahn, U.: Mesopause temperatures derived from probing the hyperfine structure of the D2 resonance line of sodium by lidar, *J. Atmos. Terr. Phys.*, 47, 499–512, 1985.

Fricke-Begemann, C., Alpers, M., and Höffner, J.: Daylight rejection with a new receiver for potassium resonance temperature lidars, *Opt. Lett.*, 27, 1932–1934, 2002.

Fritts, D. C. und Alexander, M. J.: Gravity wave dynamics and effects in the middle atmosphere, *Rev. Geophys.*, 41, 1, 1003, doi: 10.129/2001RG000106, 2003.

Fujiwara, M., Shibata, T., and Hirono, M.: Lidar observation of sudden increase of aerosols in the stratosphere caused by volcanic injections – II. Sierra Negra event, *J. Atm. Terr. Phys.*, 44, 811–818, 1982.

Hauchecorne, A. and Chanin, M.-L.: Density and temperature profiles obtained by lidar between 35 and 70 km, *Geophys. Res. Lett.*, 7, 565–568, 1980.

Thome, K., Biggar, S., and Slater, P.: Algorithm Theoretical Basis Document for ASTER Level 2B1 – Surface radiance and ASTER Level 2B5 – Surface Reflectance, Remote Sensing Group of the Optical Sciences Center, University of Arizona, ATBD-AST-04, 45, http://eospsoc.gsfc.nasa.gov/eos_homepage/for_scientists/atbd/docs/ASTER/atbd-ast-04.pdf, 1999.

Vaughan, G., Wareing, D. P., Pepler, S. J., Thomas, L., Mitev, V. M.: Atmospheric temperature measurements made by rotational Raman scattering, *Appl. Opt.*, 32, 2758–2764, 1993.

von Zahn, U. and Höffner, J.: Mesopause temperature profiling by potassium lidar, *Geophys. Res. Lett.*, 23, 141–144, 1996.

Zuev, V. V., Burlakov, V. D., El'nikov, A. V., Ivanov, A. P., Chaikovskii, A. P., and Shcherbakov, V. N.: Processes of long-term relaxation of stratospheric aerosol layer in northern hemisphere after a powerful volcanic eruption, *Atmos. Env.*, 35, 5059–5066, 2001.

Temperature lidar measurements

M. Alpers et al.

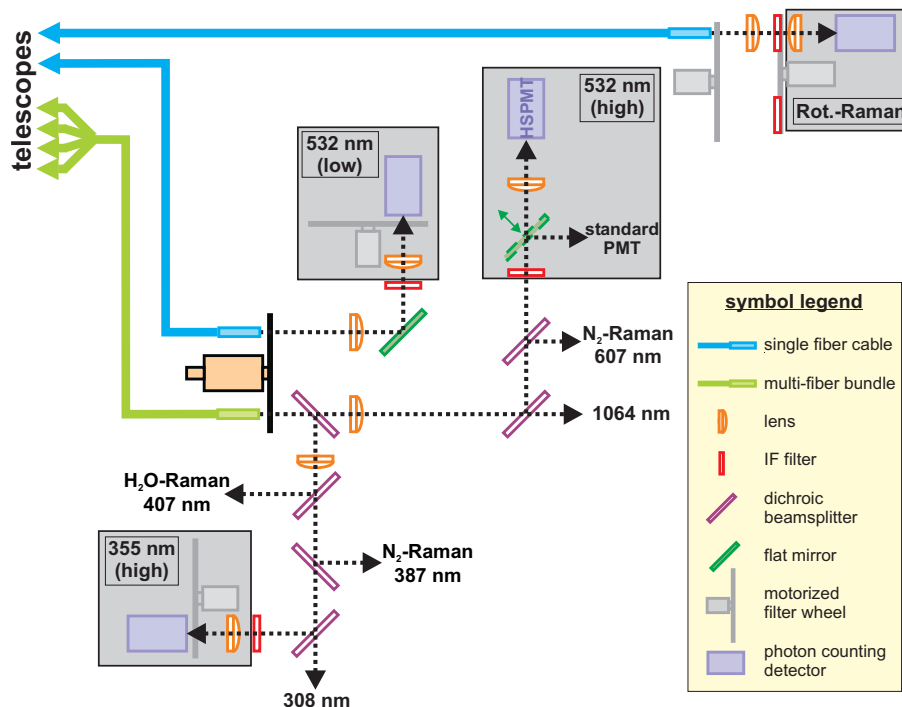


Fig. 1. Re-arranged detection system of the IAP RMR lidar at Kühlungsborn, Germany. The detectors “532 nm (low)” and the high sensitivity photomultiplier (HSPMT) of “532 nm (high)” are used for lower and higher altitude Rayleigh measurements, respectively. The standard 355 nm (high) detector is used for redundancy with the 532 nm (high) HSPMT only. The “Rot.-Raman” detector for Rotational Raman temperature measurements contains only one PMT with an interference filter wheel in front of it. This allows alternating measurements of the two Rotational Raman wavelengths as described in the text. The detector also includes additional Raman detector channels. These are of no importance for the temperature measurements of this work and therefore they are not shown in detail.

Title Page

Abstract

Introduction

Conclusions

References

Tables

Figures

◀

▶

◀

▶

Back

Close

Full Screen / Esc

Print Version

Interactive Discussion

Temperature lidar measurements

M. Alpers et al.

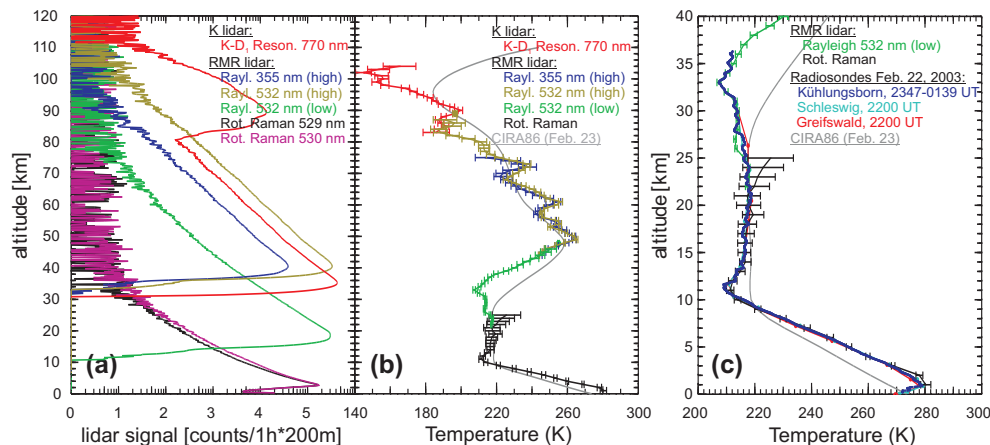


Fig. 2. Example of a temperature lidar measurement with the IAP lidars at Kühlungsborn, Germany on 23 February 2003 at 00:30–01:30 UT. Panel (a) shows the (background-corrected) raw lidar backscatter profiles of the different lidars and detectors. Panel (b) shows the temperature profiles, calculated from the raw data of panel (a). A smooth filter (0.6–3 km width, depending on altitude) and the corrections mentioned in the text have been applied. Panel (c) shows the same time period as panel (b) but limited to the altitude range 0–40 km. In addition to the lidar data temperature profiles of three radiosondes are shown. One radiosonde was launched at 23:47 UT at Kühlungsborn (blue line) and two radiosondes were launched at about 22:00 UT at the DWD stations Schleswig and Greifswald (light blue and red lines).

Title Page

Abstract

Introduction

Conclusions

References

Tables

Figures

◀

▶

◀

▶

Back

Close

Full Screen / Esc

Print Version

Interactive Discussion

© EGU 2004

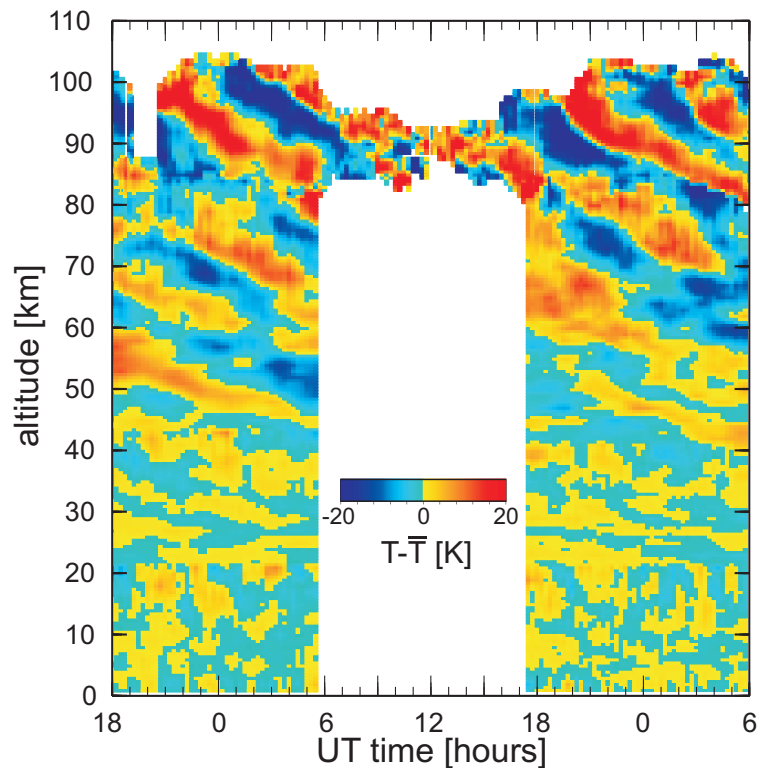


Fig. 3. Color-coded temperature deviation from the altitudinal mean for the time period between 22 February 2003, 18:00 UT and 24 February 2003, 06:00 UT, measured with the combined IAP lidars. The profiles are calculated every 15 min with a 1 h running mean. The potassium resonance lidar detector is equipped with a narrow filter for daytime measurements, while Rayleigh and Rotational Raman temperature measurements are possible only during nighttime.

Temperature lidar measurements

M. Alpers et al.

Title Page

Abstract

Introduction

Conclusions

References

Tables

Figures

◀

▶

◀

▶

Back

Close

Full Screen / Esc

Print Version

Interactive Discussion